J|A|C|S
ARTICLES
Published on Web 08/17/2006

Molecular Structure and Dynamics at the Interfaces within Bulk Heterojunction Materials for Solar Cells

Cuiying Yang,† Jerry G. Hu,‡ and Alan J. Heeger*,†

Contribution from the Center of Polymers and Organic Solids, University of California, Santa Barbara, California 93106-5090 and Materials Research Laboratory, University California, Santa Barbara, California 93106-5121

Received May 26, 2006; E-mail:

Abstract: The molecular structures within the interfaces of the bulk heterojunction material comprising regioregular-poly(3-hexylthiophene-2,5-diyl), rrP3HT, and C_{60} or its soluble derivative, [6,6]-phenyl-C_{61}-butyric acid methyl ester, PCBM, have been studied by one- and two-dimensional nuclear magnetic resonance (NMR). The local structure within the interface was inferred from chemical shift (CS) data obtained from composite films (CFs) fabricated at room temperature (PCBMCF-RT and C_{60}CF-RT) and from CFs that had been subsequently annealed at 150 °C for 30 min (PCBMCF-A150 and C_{60}CF-150A). In PCBMCF-RT, the alkyl side chains of rrP3HT are close to the C_{60} ball; C_{60} is essentially 'wrapped' by the alkyl side chains. In PCBMCF-A150, the alkyl side chains self-assemble such that rrP3HT and PCBM are separated. The observation of well-defined splittings in the CS spectrum of the ^{13}C of C_{60} in C_{60}CF-A150 indicates a distortion from spherical symmetry. Measurements of the spin−lattice relaxation rate, $1/T_1$, of C_{60} imply local magnetic field fluctuations that arise from the dynamics of the C_{60} distortion.

Introduction

Polymer-based bulk heterojunction materials have attracted attention because of the promise of low-cost solar cells fabricated by printing and coating technology.[1−10] In particular, photovoltaic cells fabricated with phase-separated composites of rrP3HT and PCBM as the charge-separating and charge-transporting layer have been intensively studied.

Enhanced efficiencies have been reported after annealing at high temperatures (e.g., 5% power conversion efficiencies were achieved after annealing at 150 °C[8,9]). To understand and optimize the efficiency, microstructures of the bulk heterojunction films have been studied before and after annealing using transmission electron microscopy, TEM, X-ray diffraction, and atomic force microscopy.[7−9,11−18] The results of studies of the morphology of polymer/fullerene bulk heterojunction solar cells have been recently summarized.[19] TEM micrographs show that films fabricated at room temperature, PCBMCF-RT, and films that were subsequently annealed at 150 °C, PCBMCF-A150, are composed of nice bicontinuous interpenetrating networks, as shown in Figure 1.

Although evidence of demixing and ripening of the phase-separated composite is clearly seen, there is no information available regarding the structure of the interfaces at the molecular level. Specifically, it is important to know the local structure of the component molecules in the interfaces in the composite film and how the local structure changes after annealing. We addressed and clarified the local structure by utilizing the chemical shift data obtained through one-dimensional (1D) and two-dimensional (2D) NMR. NMR is a powerful tool for molecular structure analysis. Heteronuclear correlation (HETCOR) NMR spectroscopy correlates the ^1H and ^{13}C resonances, presented as a 2D spectrum, and structural information about the proximity of specific ^1H and ^{13}C nuclei via their dipole−dipole coupling. In addition, NMR relaxation rate data, $1/T_1$ where T_1 is the spin−lattice relaxation time,

† Center of Polymers and Organic Solids.
‡ Materials Research Laboratory.

(1) Sacriciftci, N. S.; Smilowitz, L.; Heeger, A. J.; Wudl, F. *Science* **1992**, *258*, 1474−1476.
(2) Yu, G.; Gao, J.; Hummelen, J. C.; Wudl, F.; Heeger, A. J. *Science* **1995**, *270*, 1789−1791.
(3) Shaheen, S. E.; Brabec, C. J.; Sariciftci, N. S.; Padinger, F.; Fromherz, T.; Hummelen, J. C. *Appl. Phys. Lett.* **2001**, *78*, 841−843.
(4) Padinger, F.; Rittberger, R. S.; Sariciftci, N. S. *Adv. Funct. Mater.* **2003**, *13*, 85−88.
(5) Al-lbrahim, M.; Ambacher, O.; Sensfuss, S.; Gobsch, G. *Appl. Phys. Lett.* **2005**, *86*, 201120−3.
(6) Kim, Y.; Choulis, S. A.; Nelson, J.; Bradley, D. D. C.; Cook, S.; Durrant, J. R. *Appl. Phys. Lett.* **2005**, *86*, 063502−3.
(7) Savenije, T. J.; Kroeze, J. E.; Yang, X.; Loos, J. *Adv. Funct. Mater.* **2005**, *15*, 1260−1266.
(8) Ma, W.; Yang, C.; Gong, X.; Lee, K.; Heeger, A. J. *Adv. Funct. Mater.* **2005**, *15*, 1617−1622.
(9) Reyes-Reyes, M.; Kim, K.; Carroll, D. L. *Appl. Phys. Lett.* **2005**, *87*, 083506−3.
(10) Xue, J.; Rand, B. P.; Uchida, S.; Forrest, S. R. *J. Appl. Phys.* **2005**, *98*, 124903−9.
(11) Kline, R. J.; Mcgehee, M. D.; Toney, M. F. *Nat. Mater.* **2006**, *5*, 222−228.
(12) Sivula, K.; Ball, Z. T.; Watanabe, N.; Frechet, J. M. J. *Adv. Mater.* **2006**, *18*, 206−210.
(13) Reyes-Reyes, M.; Kim, K.; Dewald, J.; Lopez-Sandoval, R.; Avadhanula, A.; Curran, S.; Carroll, D. *Org. Lett.* **2005**, *7*, 5749−5752.
(14) Zhokhavets, U.; Erb, T.; Hoppe, H.; Gobsch, G.; Sariciftci, N. S. *Thin Solid Film* **2006**, *496*, 679−682.
(15) Huang, J.; Li, G.; Yang, Y. *Appl. Phys.* **2005**, *87*, 112105−3
(16) Inoue, K.; Ulbricht, R.; Madakasira, P. C.; Sampson, W. M.; Lee, S.; Gutierrez, J.; Ferraris, J.; Zakhidov, A. A. *Synth. Met.* **2005**, *154*, 41−44.
(17) Camaioni, N.; Ridolfi, G.; Casalbore-Miceli, G.; Possamai, G.; Maggini, M. *Adv. Mater.* **2002**, *14*, 1735−1738.
(18) Yang, X.; Van Duren, J. J. K.; Jassen, R. A. J.; Michels, M. A. J.; Loobs, J. *Macromolecules* **2004**, *37*, 2151−2158.
(19) Hoppe, H.; Saricitfci, N. S. *J. Mater. Chem.* **2006**, *16*, 45−61.

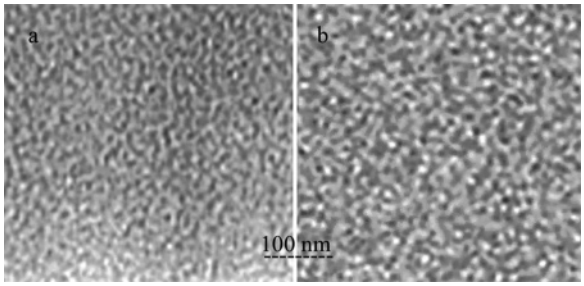

Figure 1. TEM picture of PCBMCF-RT (a) and PCBMCF-A150 (b) showing the bicontinuous interpenetrating network of the composites.

provide information on the molecular dynamics in the solid state.[20−24]

The molecular structure of pure C_{60} is like that of a soccer ball.[25] NMR studies showed that the pure C_{60} molecule has a single sharp line in the CS spectrum, thus demonstrating that all carbon atoms are chemically equivalent and implying that the structure must necessarily have icosahedral symmetry (pseudo-spherical symmetry).[26,27] However, the symmetry of C_{60} is sensitive to its environment. For example, distortions from spherical symmetry have been inferred for C_{60} in solvent,[28] on gold surfaces,[29] or in PMMA.[30] In its ground state, neutral C_{60} possesses a closed-shell electronic structure, and thus, Jahn−Teller distortion is not expected. However, because the C_{60} LUMO is 3-fold degenerate, Jahn−Teller distortion would be expected for C_{60}^- anions or C_{60} in its lowest energy excited state.[31−35]

In this paper, we report the results of NMR studies of PCBMCF-RT, PCBMCF-A150, C_{60}CF-RT, and C_{60}CF-A150 with the goal of obtaining information on the local molecular structure and intermolecular dynamics within and near the interfaces of the phase-separated material in order to better understand the photoinduced charge separation in bulk heterojuntion solar cells. Although use of a number of solvents has been described in the literature, there are differences in the nano- or mesostructure, e.g., the crystallinity, domain size, and morphology of the films, from these different solvents as summarized in ref 19. This is the reason the use of different solvents results in different device performance. In this initial but thorough and detailed NMR study we prepared the composite material in a manner identical to that used in fabricating the best devices that have been reported in the literature as described in ref 8.

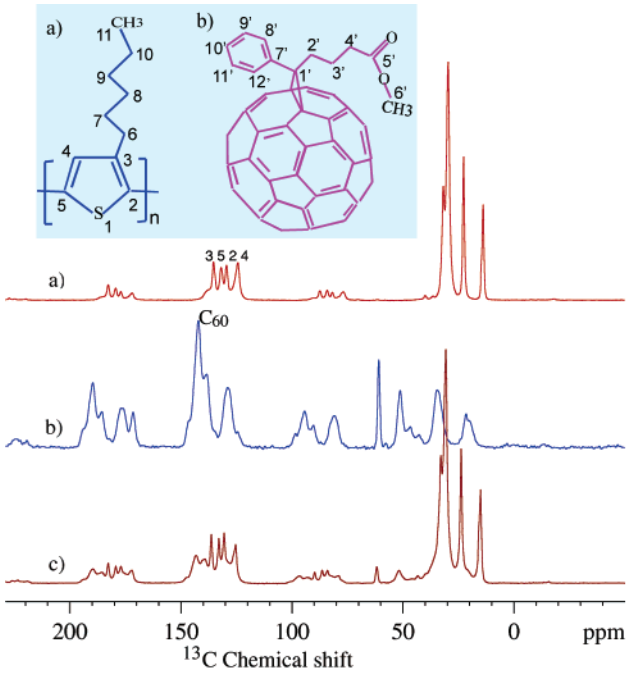

Figure 2. (a, b, and c) 1D ^{13}C NMR spectra of P3HT, PCBM, and PCBMCF-RT, respectively. The sketches of the molecules with carbon numbers of rrP3HT (a) and PCBM (b) are shown in inset.

We find that in PCBMCF-RT the long alkyl side chains of rrP3HT are close to and in effect 'wrap' the C_{60} ball in the interfaces within the bicontinuous interpenetrating network. In the PCBMCF-A150 film, the alkyl side chains of rrP3HT self-assemble such that the rrP3HT and PCBM molecule are separated from each other. The detailed changes in local structure obtained from the NMR data are consistent with the more complete phase separation and improved structural order observed by transmission electron microscopy and X-ray diffraction after annealing. Similar local structures are inferred for C_{60}CF-RT and C_{60}CF-A150. Moreover, the chemical shift data provide direct evidence that the carbon atoms of C_{60} in the annealed composites are *chemically inequivalent*, implying a distortion of the molecular structure likely driven by the breaking of the 3-fold degeneracy of the C_{60} LUMO energy levels as in the Jahn−Teller effect.[31] The spin−lattice relaxation rate, $1/T_1$, of C_{60} in PCBMCF-A150 is a factor of 2 higher than that in PCBMCF-RT, implying dynamic fluctuations of the distorted C_{60}.

Experimental Methods

rrP3HT, PCBM, and C_{60} were purchased from Aldrich (the Rieke specialty semiconducting polymer), Organic Vision Inc., and Bucky-USA, respectively, and used without purification. The chemical structures of the rrP3HT and PCBM molecules are shown in insets a and b in Figure 2.

Samples for TEM were prepared by putting a drop of 1% (w/v) mixed solution in chlorobenzene, 1:1 (w/w) of rrP3HT and PCBM on TEM grids, and dried in a slow N_2 stream. The film thickness was approximately 100 nm. To obtain such thin films it is necessary to control the amount of solution on the grid. We used filter paper to absorb the solution away if there was more than needed on the grid.

(20) Duer, M. J. *Solid-state NMR spectroscopy, principle and application*; Blackwell Science, Inc.: Malden, 2002.
(21) Ernst, R. R.; Bodenhausen, G.; Wokaun, A. *Principles of nuclear magnetic resonance in one and two dimensions*; Clarendon: Oxford, 1987.
(22) Pine, A.; Ruben, D. J.; Vega, S.; Mehring, M. *Phys. Rev. Lett.* **1976**, *36*, 110−113.
(23) Bakhnutov, V. I. *Practical NMR relaxation for chemists*; John Wiley & Sons Ltd.: New York, 2004.
(24) Spiess, H. W. *NMR: Basic Principles and Progress*; Springer-Verlag: New York, 1978; *15*, 55.
(25) Kroto, H. W.; Heath, J. R.; O'Brien, S. C.; Curl, R. F.; Smalley, R. E. *Nature* **1985**, *318*, 162−163.
(26) Johnson, R. D.; Meijer, G.; Bethune, D. S.*J. Am. Chem. Soc.* **1990**, *112*, 8983−8984.
(27) Tycko, R.; Haddon, R. C.; Dabbagh, G.; Glarum, S. H.; Douglass, D. C.; Mujsce, A. M. *J. Phys. Chem.* **1991**, *95*, 518−520.
(28) **)** Gallagher, S. H.; Armstrong, R. S.; Clucas, W. A.; Lay, P. A.; Reed, C. A. *J. Phys. Chem.* **1997**, *A 101*, 2960−2968.
(29) Garrell, H. L.; Herne, T. M.; Szafranski, C. A.; Diederich, F.; Ettl, F.; Whetten, R. L. *J. Am. Chem. Soc.* **1991**, *113*, 6302−6303.
(30) Ohta, N.; Tanaka, T.; Yamazaki, I. *Res. Chem. Intermed.* **2001**, *27*, 61−71.
(31) O'Brien, M. C. M.; Chancey, C. C. *Am. J. Phys.* **1993**, *61*, 688−697.
(32) Ostling, D.; Rosen, A. *Chem. Phys. Lett.* **1993**, *202*, 389−393.
(33) de Coulon, V.; Martins, J. L.; Reuse, F. *Phys. Rev.* **1992**, *B 45*, 13671−13675.
(34) Negri, F.; Orlandi, G.; Zerbetto, F. *Chem. Phys. Lett.* **1988**, *144*, 31−37.
(35) Morita, S.; Zakhidov, A. A.; Yoshino, K. *Solid State Commun.* **1992**, *82*, 249.

The prepared TEM samples (on the TEM grids) were placed in an oven filled with N_2 gas, and the sample was annealed at 150 °C for 30 min followed by slowly cooling to RT after turning off the power. TEM pictures were taken in a JEM 1230 electron microscope (80 kV).

For the NMR experiments, the PCBMCF-RT and C_{60}CF-RT samples were prepared by drop casting 2% mixed solution in chlorobenzene, 1:1 (w/w) of rrP3HT and PCBM (or rrP3HT and C_{60}) on glass slides (1×3 in.^{2}/each). Typically, around 5 mL of mixed solution was used for drop casting onto large area glass slides (1×3 in.^{2}/each). Several slides were used at once and dried in N_2 stream. The thickness of the drop cast film was several hundred nanometers to approximately 1 μm. The composite material was collected after drying in a slow N_2 stream overnight and at least for another 2 days drying in N_2 before use in NMR. The film was peeled off using a sharp blade. Approximately 100 mg of the composite material was packed into a NMR rotor. The PCBMCF-A150 and C_{60}CF-A150 samples were prepared by annealing PCBMCF-RT and C_{60}CF-RT in N_2 at 150 °C for 30 min (the samples were annealed in the NMR rotor without a cap) after completing NMR measurements at RT. The same annealing procedure was carried out for the pure C_{60} sample.

Samples of rrP3HT in solution in $CDCl_3$ (2% (w/v)) were prepared while stirring for several hours at 40 °C on a hot plate and subsequently used at RT for solution NMR.

In the following, the abbreviations or acronyms are as follows: TPPM is two-pulse phase modulation; CP-MAS is cross polarization magic-angle spinning; ^{1}H HSQCGP is heteronuclear singlebond quantum correlation grid pulse program, the correlation via ^1J(H, C) coupling and ^{1}H HMBCGP the heteronuclear multiple bond grid pulse program, the correlation via ^2J(H,C) and ^3J(H,C) coupling, respectively; 2D ^{13}C{^{1}H} HETCOR stands for two-dimenssional ^{13}C and ^{1}H heteronuclear correlation.

A Bruker 500 MHz Avance spectrometer (11.7 T) with a 4 mm broadband magic angle spinning (MAS) probe doubly turned to ^{1}H (500.1 MHz) and ^{13}C (125.8 MHz) was used for the solid-state and solution NMR measurements. The solid-state ^{13}C NMR spectra of pristine rrP3HT, pristine PCBM, and their composite films of PCBMCF-RT and PCBMCF-A150 were acquired using TPPM and ^{1}H decoupling, ramp CP-MAS techniques with a spin speed of 6 kHz, recycling delay time of 6 s, and contact time of 8 ms. The solid-state ^{1}H NMR spectra of rrP3HT and PCBM were acquired using the ^{1}H MAS technique at a spin speed 12 kHz. The solution ^{1}H{^{13}C} correlation NMR spectra of the solution of P3HT were acquired using ^{1}H HSQCGP and ^{1}H HMBCGP, respectively. The solid-state 2D ^{13}C{^{1}H} HETCOR experiments for PCBMCF-RT and PCBMCF-A150 were carried out with TPPM and ramp CP MAS with a contact time of 8 ms during mixing, cycling delay time of 2.5 s, and spin speed of 12 kHz.

The 1D ^{13}C spectra for pure C_{60} before and after annealing were obtained with MAS (TPPM) with a spin speed of 6 kHz and delay time of 10 s. The 1D ^{13}C experiments for C_{60}CF-RT and C_{60}CF-A150 were carried out with ramp CP MAS (TPPM) and a contact time of 5 ms at a spin speed of 6 kHz and delay time of 3 s. The 2D ^{13}C{^{1}H} HETCOR experiments for C_{60}CF-RT and C_{60}CF-A150 were carried out with ramp CP MAS (TPPM) and a contact time of 5 ms at a spin speed of 6 kHz and delay time of 3 s.

The ^{13}C spin−lattice relaxation time (T_1) measurements for rrP3HT, PCBM, PCBMCF-RT, and PCBMCF-A150 were carried out with the ^{13}C CP MAS pulse program with delay times of 0.01, 0.5, 5, 10, 16, 20, and 30 s. The spin speed was 7 kHz.

Results and Discussion

1. Molecular Structure at the Interfaces within the Bicontinuous Interpenetrating Networks of PCBMCF-RT and PCBMCF-A150 Materials. 1.1. ^{13}C Assignments. Figure 2 shows 1D ^{13}C solid-state NMR spectra of (a) pure rrP3HT, (b) pure PCBM, and (c) PCBMCF-RT obtained using the CP-MAS technique. Note that all 1D or 2D NMR spectra were obtained from solid samples unless otherwise stated. The four peaks at chemical shift (CS) values of 136, 133, 130, and 125 ppm can be assigned to the C-3, C-5, C-2, and C-4 thiophene carbons, respectively (the numbers are indicated in inset a of Figure 2), using ^{1}H HSQCGP and ^{1}H HMBCGP pulse programs for the 2% (w/v) P3HT solution in $CDCl_3$ (the 2D solution spectra are not included here). By using the ^{1}H HSQCGP program the correlation of C-4 with the attached single-bonded proton can be detected via ^1J(C, H) coupling. By using the ^{1}H HMBCGP program the correlation of the C-5, C-2, and C-3 carbons with multiple-bonded protons can be detected via ^2J(C, H) and ^3J(C, H) coupling.

The resulting assignments of the four peaks are indicated on the rrP3HT spectrum shown in Figure 2a. The peaks in the 32−10 ppm region can be assigned to the carbons of the rrP3HT alkyl side chains; these assignments are based upon calculation using ACD/NMR (v. 9.20) software together with information contained in the refs 36−37. The remaining small peaks in Figure 2a are sidebands that arise from the anisotropy of the nuclear spin−spin interactions in the solid state.

Figure 2b shows the 1D ^{13}C NMR spectrum of PCBM. The peaks at 172, 143, and 139 ppm can be assigned to C-5′, C60, and C-7′, respectively. Note that the peak at 139 ppm may result in part from the overlap of chemical shifts of C-7′ and C_{60}, i.e., part of the 139 ppm peak may originate from the C atoms of C_{60} since the C_{60} peak is quite broad. The broad peak at ∼130 ppm results from the overlap of the contributions from the aromatic carbons C-8′, C-9′, C-10′, C-11′, and C-12′. The peaks at 62, 52, 35, and 24 ppm can be assigned to C-6′, C-1′, C-4′, and C-2′,3′, respectively. The PCBM carbon label numbers are indicated in inset b of Figure 2. The remaining peaks are, again, the sidebands. These assignments of the CS peaks of PCBM carbons were made using ACD/NMR(v.9.20) software calculations together with information in the refs 26, 27, 36, and 37.

Figure 2c shows the 1D ^{13}C NMR spectrum of the PCBMCF-RT material. Comparing Figure 2c to 2a and 2b, one sees that the ^{13}C peaks of the composite PCBMCF-RT material are a superposition of those from rrP3HT (Figure 2a) and PCBM (Figure 2b). This implies that the CSs of the carbons do not change significantly in the composite materials relative to those in the pure components. Note that because the peaks in the solid-state NMR are relatively broad, the error in all assignments is ≤1 ppm. The 1D ^{13}C spectra of PCBMCF-RT and PCBMCF-A150 before and after annealing, respectively, are not distinguishable within experimental error. The peak numbers and CSs of the corresponding carbons of the composite films are listed in the first, second, and third columns of Table 1.

1.2. ^{1}H Assignments. Figure 3a and 3b are 1D NMR spectra of the ^{1}H of pure P3HT and pure PCBM, respectively. The weak and strong peaks at 6.5 and 1.0 ppm in Figure 3a can be assigned to ^{1}H on C-4 of the thiophene ring and ^{1}H on the alkyl side chains of P3HT (see inset a of Figure 2). The peaks at 7.5 and 3.6 ppm and the shoulder at 2.4 ppm in Figure 3b can be assigned to the ^{1}H on the phenyl, methoxy, and methylene groups of PCBM (see inset b of Figure 2), respectively. Note that there is almost no peak at the 1.0 ppm position in the PCBM spectrum of Figure 3b.

(36) Dean, J. A. *Handbook of Organic Chemistry*; McGraw-Hill Book Co.: New York, 1987; pp 6-68−6-90.
(37) Bruker Almanac 1999.

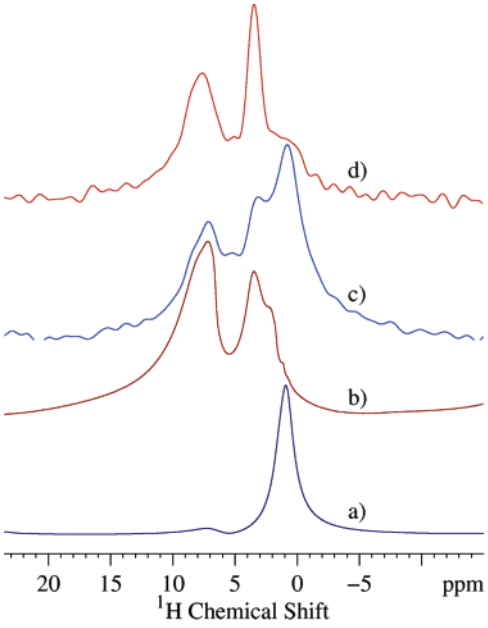

Figure 3. 1D ^{1}H spectra of P3HT (a) and PCBM (b). (c and d) 1D ^{1}H spectra obtained as slices from the 2D spectra (Figure 4a and 4b) of PCBMCF-RT (c) and PCBMCF-A150 (d) corresponding to the 143 ppm CS of C_{60}.

Table 1. Chemical Shifts and Spin−Lattice Relaxation Rates of the ^{13}C

	PCBMCF-R T and PCBMCF-A150		P3HT	PCBM	PCBMCF-RT	PCBMCF-A150
no.	CS (ppm)	assignment	$1/T_1$ (s^{-1})	$1/T_1$ (s^{-1})	$1/T_1$ (s^{-1})	$1/T_1$ (s^{-1})
1	173	C═O-5′		0.12	0.18	0.18
2	143	C_{60}		0.01	0.02	0.04
3	139	C-7′		0.03	0.06	0.1
4	136	C-3	0.1		0.09	0.09
5	133	C-5	0.06		0.08	0.07
6	130	C-2, C-9′,9′,10′,11′,12′	0.05	0.21	0.08	0.08
7	125	C -4	0.15		0.14	0.14
8	62	O-CH_3-6′		0.04	0.05	0.05
9	52	CH_2 -1′		0.14	0.21	0.2
10	35, 33	C-4′, CH_2-9	1.81		1.67	1.82
11	31	CH_2-6,7,8	2.08		1.93	2.13
12	24,22	CH_2-10, CH_2-2′,3′	1.35		1.33	1.37
13	16	CH_3-11	0.63		0.64	0.65

1.3. 2D ^{13}C{^{1}H} HETCOR Experiments for PCBMCF-RT and PCBMCF-150A. The 2D ^{13}C{^{1}H} HETCOR measurements were carried out to characterize the through-space proximity between ^{13}C and ^{1}H in the phase-separated materials (PCBMCF-RT and PCBMCF-150A) via heteromolecular correlation of ^{13}C and ^{1}H.

We focus *mainly* on the analysis of the correlation of ^{13}C from C_{60} of PCBM with ^{1}H of P3HT since we are interested in the spatial proximity of the two components at the interfaces within the phase-separated structure.

Figure 4a and 4b shows the 2D ^{13}C{^{1}H} heterocorrelation patterns of PCBMCF-RT and PCBMCF-150A, respectively. In Figure 4a the strongest peaks are at the intersections of the CS of the ^{13}C of C_{60} (143 ppm) with the CS of the ^{1}H in the alkyl side chains (1.0 ppm). This can be viewed more clearly in Figure 3c, which is a 1D spectrum sliced from Figure 4a at CS =143 ppm characteristic of C_{60}. The three principal peaks are at 7.5, 3.6, and 1.0 ppm. Note that the strongest peak at 1.0 ppm in PCBMCF-RT, shown in Figure 3c, is very weak in Figure 3b for PCBM. By comparing Figure 3c to 3a and 3b, the strongest

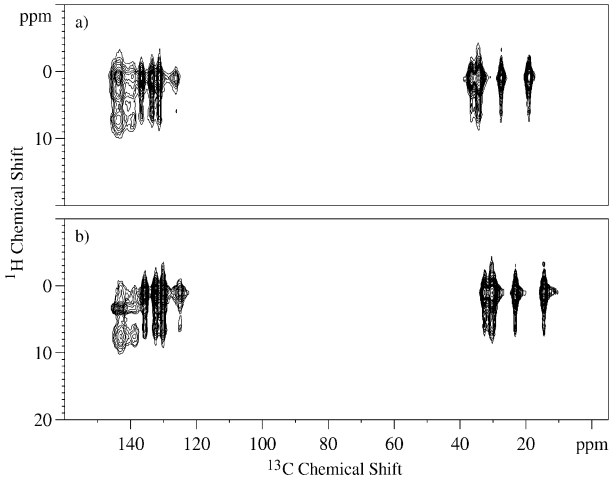

Figure 4. 2D ^{13}C{^{1}H} HETCOR spectra of PCBMCF-RT (a) and PCBMCF-150A (b) respectively.

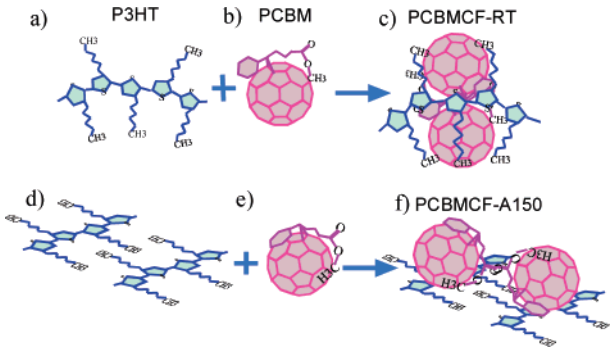

Figure 5. Illustrations of the molecular structure near the interface before (a−c) and after (d−f) annealing.

peak at 1.0 ppm in Figure 3c can be attributed to the contribution of ^{1}H from the alkyl side chains of P3HT via their strong correlation with C_{60}. In other words, C_{60} is in close spatial proximity with the alkyl side chains of P3HT after casting from solution at RT. At the interface, therefore, the C_{60} ball is close to and essentially 'wrapped' by the alkyl side chains of P3HT, as shown schematically in Figure 5a−c. The other two cross-peaks at 7.5 and 3.6 ppm as well as the shoulder at 2.4 ppm in Figure 3c result from correlation of C_{60} with the side chains of PCBM (the phenyl, methoxy, and methylene groups).

In the data from PCBMCF-150A shown in Figure 4b there are two strong cross-peaks at 7.5 and.3.6 ppm on the ^{1}H axis and 143 ppm CS of the ^{13}C axis. These can also be seen in the 1D sliced spectrum (Figure 3d) from Figure 4b at the 143 ppm CS of the ^{13}C of C_{60}. The strongest peak at 1.0 ppm in Figure 3c becomes very weak (only a shoulder) in Figure 3d. This implies that correlation of C_{60} with the ^{1}H of the alkyl side chains of P3HT becomes very weak. Thus, the alkyl side chains are no longer in close proximity with C_{60}; demixing occurs after annealing at 150 °C

In the PCBMCF-150A material, after annealing at 150 °C, the alkyl side chains are strongly intercorrelated, implying interdigitated self-assembly as sketched in Figure 5d. The C_{60} becomes more strongly correlated with its own side chain, especially with the methoxy group of PCBM (see Figure 3d; the strongest cross-peak is at 3.6 ppm). Because of this self-assembly, P3HT and PCBM are separated one from other while becoming individually more ordered after annealing. This is

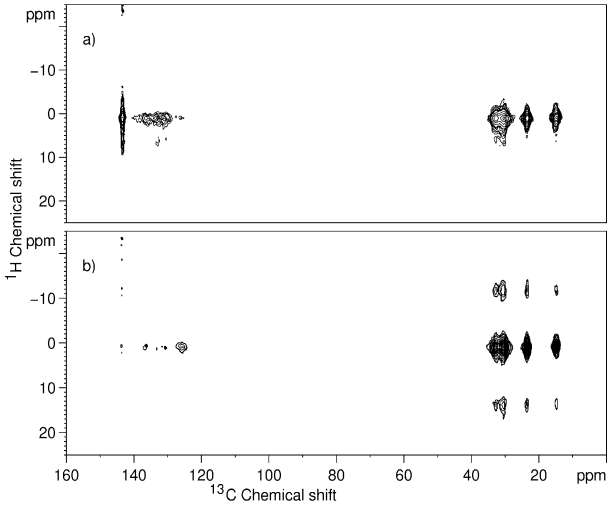

Figure 6. 2D $^{13}C\{^{1}H\}$ HETCOR spectra of C_{60}CF-RT (a) and C_{60}CF-150A (b).

consistent with the X-ray diffraction data, which shows that the alkyl side chains exhibit improved structural order (the diffraction peak that arises from the 1.62 nm *d* spacing associated with the interdigitated alkyl side chains increases in intensity[8]). Note that this evidence of self-assembly in PCBMCF-A150 implies that the interaction between the alkyl side chains is stronger than that between the side chains and C_{60}. Apparently, formation of the 'wrapped' structure shown in Figure 5c is not the lowest energy structure in the solid state but is frozen in when the composite film is cast from solution. After annealing, the PCBM molecules at the interface (Figure 5f) are in proper closer proximity to the thiophene rings. Figure 5f suggests a better-defined heterojunction at the interface with correspondingly improved photoinduced charge separation.

2. Molecular Structure at the Interfaces in C_{60}−P3HT Composites. The 2D $^{13}C\{^{1}H\}$ HETCOR spectra for C_{60}CF-RT and C_{60}CF-A150 are shown in Figure 6a and 6b. One sees a very strong cross-peak (barlike dark contour) centered at the intersection of 143.5 and 1 ppm on the left side in Figure 6a and a weak cross-peak (small spot) on the left side in Figure 6b at the same intersection as in Figure 6a. This significant difference can also be seen in the 1D ^{13}C spectra of C_{60}CF-RT and C_{60}CF-A150, as shown in Figure 7a and 7b. There is a very strong peak in Figure 7a and very weak peak in Figure 7b at CS =143.5 ppm

The strong cross-peak in 2D (Figure 6a) and strong peak in 1D (Figure 7a) imply that there is a strong proton−carbon ($^{1}H-^{13}C$) dipolar coupling between the ^{1}H of the alkyl side chains of P3HT and the ^{13}C of C_{60}, consistent with the wrapping of C_{60} by the alkyl side chains in C_{60}CF-RT, as sketched in Figure 8a−c.

The $^{1}H-^{13}C$ coupling becomes very weak in C_{60}CF-A150 (Figures 6b and 7b), implying that the alkyl side chains move away from C_{60} as described above. Thus, rrP3HT and C_{60} separate and demix during annealing. The local structures within C_{60}CF-RT (Figure 8c) and C_{60}CF-A150 (Figure 8f) are similar to those of PCBMCF-RT (Figure 5c) and PCBM-A150 (Figure 5f).

3. Evidence for Distorted C_{60} Molecular Structure. In the C_{60}−P3HT composites C_{60} has a simpler NMR spectrum than that from PCBM−P3HT because of the absence of overlap of

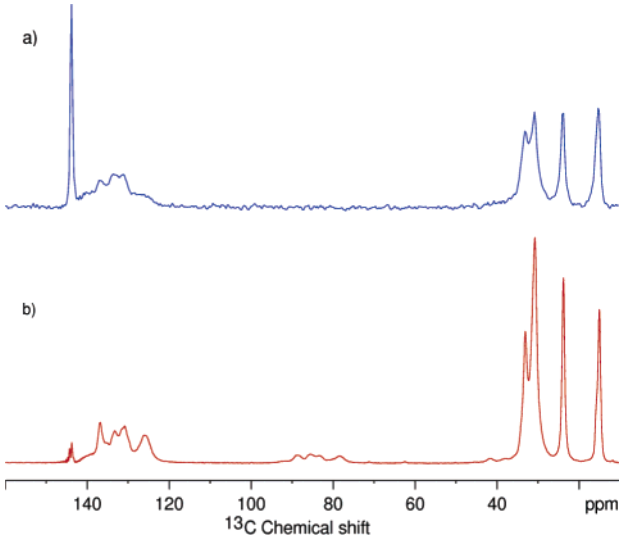

Figure 7. 1D ^{13}C spectra for C_{60}CF-RT (a) and C_{60}CF-A150 (b).

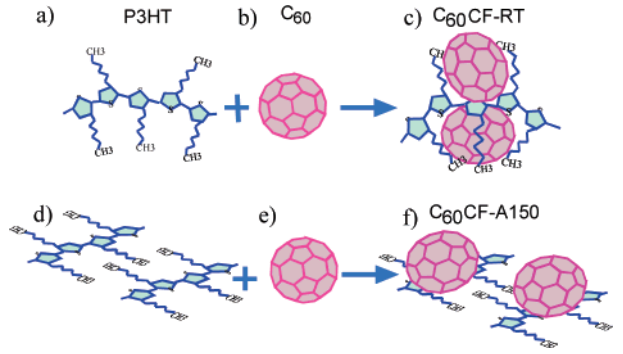

Figure 8. Schematic illustrations of wrapped C_{60} molecules by alkyl side chains in C_{60}CF-RT (a) and ordering of P3HT and C_{60} in C_{60}CF-A150 (b). Note that C_{60} is deformed in the composites.

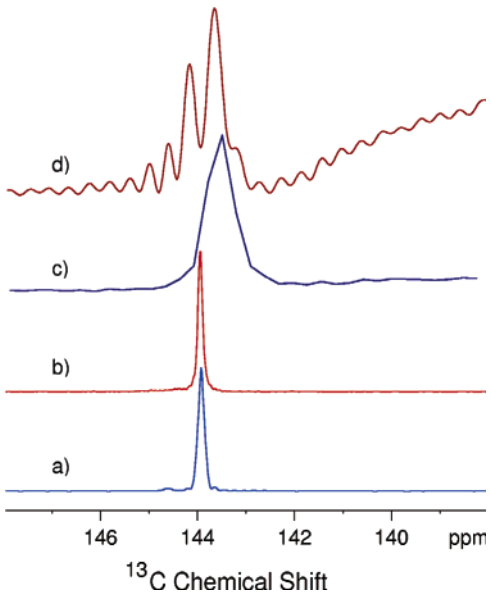

Figure 9. 1D ^{13}C spectra for pure C_{60} before (a) and after (b) annealing and for C_{60}CF-RT (c) and C_{60}CF-A150 (d).

the CS NMR peaks from the PCBM side chain. Figure 9a and b shows 1D ^{13}C MAS NMR spectra for pure C_{60} before and after annealing at 150 °C. The ^{13}C spectra in Figure 9a and 9b are identical, with a single sharp line (fwhm = 0.1 ppm) at CS

just below 144 ppm, implying that all carbon atoms of pure C_{60} are chemically equivalent and that the molecule has icosahedral symmetry as reported earlier.[25−27] Annealing at 150 °C has no effect on pure C_{60}. The corresponding 1D ^{13}C CP MAS spectra for C_{60}CF-RT and C_{60}CF-A150 are shown in Figure 9c and 9d. The single sharp ^{13}C CS peak from C_{60} becomes broad in C_{60}CF-RT (fwhm = 0.7 ppm, Figure 9c, whereas multiple peaks are clearly resolved in the ^{13}C spectrum obtained from C_{60}CF-A150 (Figure 9d). The multiple-peak spectrum obtained from C_{60}CF-A150 indicates that all carbon atoms in the C_{60} molecules are not equivalent; after annealing the C_{60}−P3HT composite at 150 °C the C_{60} molecule is distorted (as illustrated in Figure 8c and 8f), and hence, the icosahedral symmetry is broken.

The broadened CS line observed from C_{60}CF-RT does not show this clear splitting, although the spectrum can be interpreted as consisting of multiple overlapping lines. Thus, if the distortion exists in the C_{60}CF-RT material (prior to high-temperature annealing), it is reduced in magnitude from that in C_{60}CF-A150.

Note that in Figure 5c and 5f we sketched the C_{60} molecules as spheres since the splitting of the CS peak from C_{60} was not detected because of overlap of the CS peaks from the side chain of PCBM. However, since the electronic structures of C_{60} and its soluble derivative are essentially identical, we assume that the distortion is also present in the PCBMCF-A150 material.

Although the distortion of C_{60} in C_{60}CF-A150 might be interpreted as resulting from the Jahn−Teller effect,[31] we emphasize that there is no ground-state charge transfer in the C_{60}−P3HT composites. For example, the absorption spectra obtained from the C_{60}−P3HT and PCBM−P3HT composites are a simple superposition of the component spectra. According to the Jahn−Teller theorem, the distortion would be driven by the lowering of the electronic energy through splitting the 3-fold degeneracy of LUMO of C_{60}. However, there is no electronic energy gain if the LUMO is unoccupied. Mixing of the charge-transferred state into the ground state by perturbation theory could lead to a lowering of the total electronic energy analogous to the Jahn−Teller effect (second-order Jahn−Teller effect). If indeed there were some mixing of the charge-transferred state into the ground state, this would facilitate the photoinduced charge-transfer reaction. Thus, the existence of the C_{60} distortion might play a role in the increased solar cell efficiency obtained after high-temperature annealing.

In summary, for high device performance, annealing to obtain the optimized heteromolecular structure is necessary. To obtain high-efficiency solar cells, both initial charge transfer and subsequent charge separation are required. From a structural point of view, the well-defined heteromolecular structure (as described in detail above) is fundamentally important for efficient charge transfer and charge separation. The nanoscale bicontinuous interpenetrating network is ideal for achieving the highest heteromolecular interfacial area and, therefore, achieving the highest probability for charge separation. For charge transport toward the electrodes, achieving a more highly ordered structure (high crystallinity) throughout the interpenetrating network yields higher mobility. However, if the crystallites are too large, the interfacial area of the heteromolecular junctions will decrease with a corresponding decrease in the efficiency of charge separation. Therefore, optimization of these two factors is crucial.

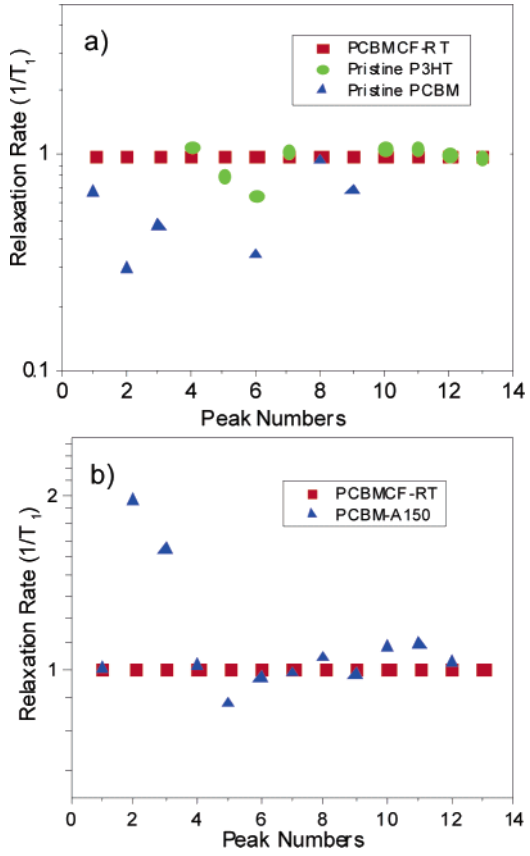

Figure 10. (a) $1/T_1$ of the carbons in P3HT (green dots), PCBM (blue triangles), and PCBMCF-RT (red squares). (b) $1/T_1$ of the carbons in PCBMCF-RT (red squares) and PCBMCF-A150 (blue triangles).

4. Spin−Lattice Relaxation Time Measurements for P3HT, PCBM, PCBMCF-RT, and PCBMCF-A150. Table 1 summarizes the ^{13}C chemical shifts and spin−lattice relaxation rates for different carbon atoms in pristine P3HT, pristine PCBM, the PCBMCF-RT material, and the PCBMCF-A150 material; the $1/T_1$ data for the ^{13}C are shown graphically in Figure 10. Note that in Figure 10 all $1/T_1$ data are normalized (for each carbon atom) with respect to the value obtained from the ^{13}C in PCBMCF-RT; i.e., $1/T_1|_{norm} = 1$. The peak numbers (no.) along the *x* axis of Figure 10 (corresponding to the different carbon atoms) are identified in the first column of Table 1.

Figure 10a shows the normalized ^{13}C relaxation rates for pristine P3HT (green dots), pristine PCBM (blue triangles), and the PCBMCF-RT material (red squares). For the carbons in the C_{60} component of PCBMCF-RT (no. 2) the rate is two times faster than that of the ^{13}C in pristine PCBM. Similarly, the relaxation rates of C-5 (no. 5) and C-2 (no. 6) in PCBMCF-RT are slightly faster than that of ^{13}C in pristine P3HT. This implies that in the PCBMCF-RT material the ^{13}C of C_{60} interact with sites C-5 (no. 5) and C-2 (no. 6) of P3HT, consistent with the structural information inferred from the chemical shift data. Figure 10b compares the rates for the various ^{13}C of PCBMCF-RT (red squares) and PCBMCF-A150 (blue triangles). For the ^{13}C of C_{60} (no. 2) $1/T_1$ is larger by a factor of 2 in PCBMCF-A150 than in PCBMCF-RT. Thus, the ^{13}C relaxation rate in C_{60} changes from $1/T_1 = 0.01$ in pristine PCBM to $1/T_1 = 0.02$

in PCBMCF-RT and to $1/T_1 = 0.04$ in PCBMCF-A150 (Table 1). The relaxation rate for the C-7′ carbon (no. 3) is also high in PCBMCF-A150 (Figure 10b). Note, however, that the ratio of the $1/T_1$ values remains nearly constant (see the actual numbers in Table 1). Thus, the increase in the rate for the C-7′ carbon probably arises from coupling between the ^{13}C on C-7′ and ^{13}C on C_{60} (see Figure 2).

Spin−lattice relaxation arises from the exchange of energy between the excited nuclear spins and their environment. This exchange of energy is mediated by local magnetic field *fluctuations* that arise from molecular motion. The relatively small changes in absolute value between the relaxation rates for the ^{13}C on C_{60} in pristine PCBM compared to that on PCBMCF-RT are consistent with the conclusion that there is no charge transfer in the ground state of the P3HT−PCBM bulk heterojunction material.

The clear observation of a distortion in the C_{60} structure as inferred from the splitting in the chemical shift spectrum (see Figures 8 and 9) suggests that the increase in the relaxation rate of ^{13}C in C_{60} in the bulk heterojunction material, especially after annealing at 150 °C, arises from fluctuations in the local structure with corresponding fluctuations in the local magnetic field via the dipole−dipole interaction between the carbon atoms of C_{60}. From the measured relaxation rates the magnitude of the power spectrum of the local magnetic field at the ^{13}C NMR frequency is largest in PCBMCF-A150.

Conclusion

In summary, the local molecular structure within the interfaces of the rrP3HT−PCBM bulk heterojunction material was inferred from chemical shift data obtained from composite material cast from solution at room temperature (PCBMCF-RT and C_{60}CF-RT) and composite material that had been subsequently annealed at 150 °C for 30 min (PCBMCF-A150 and C_{60}CF-150A). In PCBMCF-RT the alkyl side chains of rrP3HT are close to the C_{60} ball; C_{60} is essentially 'wrapped' by the alkyl side chains. In PCBMCF-A150 the alkyl side chains self-assemble such that rrP3HT and PCBM are separated. The detailed changes in local structure obtained from the NMR data are consistent with the more complete phase separation and improved structural order observed by transmission electron microscopy and X-ray diffraction after annealing. The observation of well-defined splittings in the chemical shift of the ^{13}C in C_{60} within C_{60}CF-A150 indicates a distortion from spherical symmetry. This symmetry-breaking distortion will cause an associated splitting of the 3-fold degeneracy of the LUMO of C_{60}. The spin−lattice relaxation rate of C_{60} in PCBMCF-A150 is a factor of 2 higher than that in PCBMCF-RT, implying dynamic fluctuations of the distorted C_{60}. The distortion and corresponding increase in the overlap of the excited-state wave function with the wave function of the charge-transferred state (electronic and structural) would be expected to enhance the charge-transfer rate.

Acknowledgment. This research was supported by the Heeger Center for Advanced Materials at the Gwangju Institute for Science and Technology, Gwangju, Korea.

JA063707F